DFT Study on the Ground State and Excited State Intramolecular Proton Transfer of Propargyl Arm Containing Schiff Bases in Solution and Gas Phases

ARTICLE *in* COMPUTATIONAL AND THEORETICAL CHEMISTRY · JANUARY 2013

Impact Factor: 1.55 · DOI: 10.1016/j.comptc.2013.11.018

4 AUTHORS, INCLUDING:

Annaraj Balakumaran
National Engineering College
13 PUBLICATIONS **56** CITATIONS
SEE PROFILE

Sudip Pan
IIT Kharagpur
43 PUBLICATIONS **211** CITATIONS
SEE PROFILE

M A Neelakantan
National Engineering College
60 PUBLICATIONS **451** CITATIONS
SEE PROFILE

Computational and Theoretical Chemistry 1028 (2014) 19–26

Contents lists available at ScienceDirect

Computational and Theoretical Chemistry

journal homepage: www.elsevier.com/locate/comptc

DFT study on the ground state and excited state intramolecular proton transfer of propargyl arm containing Schiff bases in solution and gas phases

B. Annaraj [a], Sudip Pan [b], M.A. Neelakantan [a,*], Pratim K. Chattaraj [b,*]

[a] Chemistry Research Centre, National Engineering College, K.R. Nagar, Kovilpatti 628 503, Thoothukudi District, Tamil Nadu, India
[b] Department of Chemistry and Center for Theoretical Studies, IIT Kharagpur, Kharagpur 721 302, India

ARTICLE INFO

Article history:
Received 27 September 2013
Received in revised form 13 November 2013
Accepted 18 November 2013
Available online 28 November 2013

Keywords:
Schiff base
Tautomerism
DFT
UV–Visible spectra
Ground state intramolecular proton transfer
Excited state intramolecular proton transfer

ABSTRACT

Electronic structure calculations on 6,6′-(1E,1′E)-1,1′-(propane-1,3-diylbis(azan-1-yl-1-ylidene))bis(ethan-1-yl-1-ylidene)bis(3-(prop-2-ynyloxy)phenol) (L1) and (E)-2-(1-(2-hydroxyethylimino)ethyl)-5-(prop-2-ynyloxy)phenol (L2) compounds are carried out at B3LYP/6-311 + G(d,p) level of theory. The enol forms are found to be more stable than the corresponding keto forms in gas phase, whereas in solvent phase the reverse is true. The computed vibrational frequencies of L1 and L2 are compared with the available experimental data. Major orbital contributions for each electronic transition are assigned with the help of time-dependent density functional theory (TD-DFT). The UV–Visible spectral data of L1 and L2 coincide with the theoretical data of keto forms, which reveal that the compounds L1 and L2 exist mostly in keto forms rather than in enol forms in solution. Potential energy curves for the intramolecular proton transfer in the ground (GSIPT) and excited (ESIPT) states are generated in gas and solution (solvent is dimethyl sulfoxide) phases. GSIPT for both L1 and L2 goes through a low activation barrier, whereas in case of ESIPT, barrierless proton transfer occurs.

1. Introduction

Schiff bases (compounds containing imine groups) are obtained by condensation of aldehydes or ketones with amines. Schiff base ligands receive significant attention due to their interesting properties, e.g., catalytic activity, selective recognition of metal ions [1], photochromic properties, antibacterial activity, and anticancer activity [2]. Schiff bases are also used as probes in investigating the structure of DNA [3]. Ligands containing propargyl functional group have a key role in neuroprotection as well as they show inhibition towards flavin-linked oxidases [4]. 10-propargyl-5,8-dideazafolate (CB3717, PDDF) is the first antifolate thymidylate synthase (TS) inhibitor which entered into clinical trials. The propargyl moiety present in the PDDF increases its potency against TS by 10-fold with respect to that of methyl analogue [5].

2-hydroxy Schiff base compounds exhibit tautomerism. Three different forms viz., enol, keto and zwitterionic forms are reported to exist in the solid state. Hydrogen bonding interaction is a matter of interest to the scientists because of its abundance in various chemical, biochemical and pharmacological systems and also due to its important role in preferential solvation [6]. The photochromism and thermochromism properties of 2-hydroxy Schiff base depend on the molecular planarity, nature of crystal packing, effect of substituent and nature of the solvent [7].

One of the fascinating topics in chemistry and biochemistry is the proton transfer reaction. A classic example is the double proton transfer between DNA base pairs [8]. Prompted by the importance of this type of reactions, both theoreticians and experimentalists have been studying the various factors associated with these processes in detail [9,10]. On the other hand, the excited state intramolecular proton transfer (ESIPT) processes get significant attention due to their different applications in the fields of ultraviolet stabilizer [11], laser dyes [12], polymer stabilizer [13], Raman filters [14], etc. For an ESIPT process, the basic mechanism involves the shifting of the proton of hydroxyl group or amino group to the intramolecular hydrogen bonded carbonyl oxygen or imine nitrogen. In this aspect, the studies on the dual emission in the fluorescence spectra of salicylic acid and methyl salicylate by Weller [15] need special mention. Theoretical investigations on ESIPT of *o*-hydroxybenzoyl [16], *o*-hydroxy Schiff bases [17] are also carried out. In a series of work, Misra et al. have studied GSIPT and ESIPT of various systems [18]. The applicability of the maximum hardness principle [19] and minimum polarizability principle [20] to locate the transition states in the potential energy curve (PEC) has also been explored [21].

* Corresponding authors.
E-mail addresses: drmaneelakantan@gmail.com (M.A. Neelakantan), pkc@chem.iitkgp.ernet.in (P.K. Chattaraj).

2210-271X/$ - see front matter © 2013 Elsevier B.V. All rights reserved.
http://dx.doi.org/10.1016/j.comptc.2013.11.018

To the best of our knowledge, there is no report available on theoretical investigation on the ground and excited state intramolecular proton transfer in Schiff bases containing the propargyl moiety. X-ray crystallographic analysis of two propargyl arm containing compounds, 6,6′-(1E,1′E)-1,1′-(propane 1,3-diyl-bis(azan-1-yl-1-ylidene))bis (ethan-1-yl-1-ylidene)bis(3-(prop-2-ynyloxy)phenol) (L1) and (E)-2-(1-(2-hydroxyethyl imino)ethyl)-5-(prop-2-ynyloxy)phenol (L2) was reported in an earlier publication [22]. The aim of the present work is to study the spectral and structural changes caused by conversion of the enol form to the keto form, using DFT. Here, we have performed the spectral characterization and theoretical investigation on the GSIPT and ESIPT of the synthesized 6,6′-(1E,1′E)-1,1′-(propane-1,3-diylbis(azan-1-yl-1-ylidene))bis(ethan-1-yl-1-ylidene)bis(3-(prop-2-ynyloxy) phenol) (L1) and (E)-2-(1-(2-hydroxyethylimino)ethyl)-5-(prop-2-ynyloxy)phenol (L2) [22].

2. Computational details

The geometry optimization of keto and enol forms as well as the transition states (TS) of L1 and L2 in gas phase is performed by carrying out density functional theory (DFT) calculations with Becke's three-parameter exchange and Lee–Yang–Parr correlation functionals (B3LYP) with a combination of 6-311 + G(d,p) basis set as implemented in Gaussian 03 suite of program [23]. GaussView program [24] is used for the visualization of the studied systems. The harmonic vibrational frequencies of the studied structures are calculated at the same level to characterize their existence on the potential energy surface (PES). The minimum energy structures are ensured by the absence of any imaginary frequency whereas any transition state is characterized by the presence of only one imaginary frequency. In solution phase, the geometry optimization of the studied structures is performed at the same level with polarizable continuum model (PCM) [25]. Electronic absorption spectra of the compounds are generated by using TD-DFT method in gas and solution phases with different solvents such as chloroform ($CHCl_3$), ethanol (C_2H_5OH) and dimethyl sulfoxide (DMSO), at the same level.

3. Results and discussion

3.1. Crystal structures and optimized geometries of L1 and L2

The optimized geometries of L1 and L2 are provided in Fig. 1. According to crystallographic data, the compounds L1 and L2 belong to triclinic crystal system with space group of $P\bar{1}$ and Pi, respectively [22]. The bond lengths and bond angles obtained from crystal data are comparable to theoretical data. The selected bond lengths and angles of L1 and L2 are given in Table 1. For L1, the experimental bond lengths of C(15)—N(2) and C(22)—O(3) are comparable with that of the enol form, obtained theoretically (Table 1). For L2 also, the experimental C(5)—O(2) and C(10)—N(1) bond lengths are equivalent to that of the enol form of the optimized geometry. The small discrepancies between the experimental and theoretical values are due to change in phase. Crystal data correspond to molecules in solid phase, whereas theoretical data correspond to molecules in gas phase. Single isolated molecule is considered in the theoretical calculations, whereas the results of X-ray study are associated with molecular packing.

The existence of hydrogen bonds in the optimized structures is observed in the O(2)—H(15)–N(1) portion of L2 and in the O(2)—H(25)–N(1) and O(3)—H(26)–N(2) portions of L1, respectively. The D (Donor)—H, H—A (Acceptor) bond distances, and <D—H–A bond angle values are 1.001 Å, 1.638 Å, and 149.38° respectively, whereas the values obtained from the X-ray study are 0.82 Å, 1.82 Å, and 148°, respectively. Similarly, for L2, the values of D—H, H—A distances, and <D—H–A bond angle in the optimized structure are 1.010 Å, 1.620 Å and 150.07°, respectively, and are comparable with the X-ray data, 0.821 Å, 1.77 Å and 148°, respectively. Even though some differences are observed, in general, the there are good matching between the calculated geometrical parameters and those obtained from the X-ray structure.

3.2. Potential energy curves (PECs) for GSIPT and ESIPT of L2 and L1

Selection of proton transfer coordinate is a crucial job for the building of ground and excited state potential energy curves (PEC). For a small system, intrinsic reaction coordinate approach (IRC) is quite handy as proton transfer reaction co-ordinate. One probable approach to generate potential energy curves for both GSIPT and ESIPT processes is to vary O(2)—H(15) distance fixing O(2)—N(1) [26]. The plots of O(2)—N(1) distance and O(2)—H(15)—N(1) angle as a function of O(2)—H(15) distance of L2 in gas and DMSO phases are given in Fig. 2. The plots clearly demonstrate that as the proton transfers from O(2) to N(1), the O(2)—N(1) distance gets noticeable change. At lesser distance, it decreases gradually and ultimately gets a minimum at O(2)—H(15) distance of 1.25 Å. Thereafter, it increases upon further increasing the O(2)—H(15) distance. The case is reverse during the change of O(2)—H(15)—N(1) angle with respect to O(2)—H(15) distance. Therefore, the freezing of the geometry of L2 or the fixing the O(2)—N(1) distance at a particular value leads to the introduction of an artificial constraint on the system. Another approach involves the consideration of O(2)—H(15) distance as proton transfer reaction co-ordinate named as 'distinguished co-ordinate approach' by Sobolewski and Domcke [27]. Catalan et al. [28], Maheswari et al. [29], and Misra et al. [18,21] also considered this approach for the GSIPT and ESIPT processes of various systems. In this study, we have generated the PEC for L2 by varying O(2)—H(15) distance from 0.9 to 1.8 Å in gas phase and from 0.9

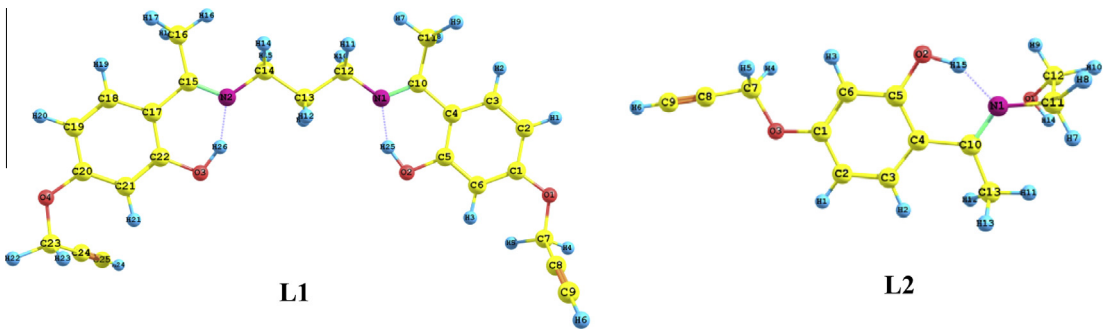

Fig. 1. Optimized structures of L1 and L2 studied at B3LYP/6-311 + G(d,p) level of theory.

Table 1
Selected bond length (Å), bond angle (°) and Torsion angle (°) of L1 and L2.

Parameters (L1)	Exp*	Computed		Parameters (L2)	Exp*	Computed	
		Enol	Keto			Enol	Keto
C(4)—C(5)	1.435	1.422	1.469	C(1)—C(6)	1.376	1.388	1.373
C(5)—O2	1.302	1.33	1.268	C(1)—C(2)	1.415	1.405	1.424
O(2)—H(25)	0.82	1.001	–	C(2)—C(3)	1.352	1.379	1.364
C(4)—C(10)	1.437	1.46	1.418	C(3)—C(4)	1.419	1.41	1.427
C(10)—N(1)	1.31	1.291	1.330	C(4)—C(5)	1.444	1.422	1.469
C(14)—N(2)	1.464	1.458	1.457	C(5)—C(6)	1.423	1.403	1.436
C(15)—N(2)	1.315	1.296	1.330	C(5)—O(2)	1.29	1.336	1.268
C(15)—C(16)	1.491	1.517	1.508	O(2)—H(15)	0.821	1.0103	1.579
C(15)—C(17)	1.439	1.47	1.418	C(4)—C(10)	1.431	1.473	1.421
C(17)—C(18)	1.419	1.412	1.416	C(10)—N(1)	1.308	1.292	1.33
C(18)—C(19)	1.357	1.381	1.365	C(11)—N(1)	1.461	1.448	1.451
C(19)—C(20)	1.4	1.408	1.427	N(1)—H(15)	–	1.620	1.053
C(20)—C(21)	1.376	1.39	1.372	C(4)—C(10)—N(1)	118.9	117.61	118.4
C(17)—C(22)	1.434	1.427	1.465	C(4)—C(5)—O(2)	122.3	122.11	122.6
C(21)—C(22)	1.402	1.406	1.437	C(10)—N(1)—H(15)	–	–	111.21
C(22)—O(3)	1.298	1.335	1.268	C(5)—O(2)—H(15)	109.4	105.37	–
O(3)—H(26)	0.82	1.012	–	C(5)—C(4)—C(10)—N(1)	0.1	−1.768	−0.286
N(1)—H(26)	–	–	1.055	C(4)—C(5)—O(2)—H(15)	0.8	1.123	–
N(2)—H(25)	–	–	1.055	C(4)—C(10)—N(1)—C(11)	−177.9	−178.16	−179.51
H(25)—O(2)—C(5)	109.5	105.56	–	N(1)–H(15)	1.77	1.62	–
C(5)—C(4)—C(10)	120.9	120.85	119.6				
C(4)—C(10)—N(1)	117.3	118.17	119.12				
C(22)—O(3)—H(26)	109.5	105.56	–				
C(21)—C(22)—O(3)	119.9	117.33	119.8				
C(17)—C(15)—N(2)	117.5	118.17	119.12				
C(16)—C(15)—N(2)	120.2	123.6	117.08				
C(15)—N(2)—H(25)	–	–	−0.442				
N(1)—C(10)—C(4)—C(3)	176.3	−179.85	−179.1				
N(1)—C(10)—C(4)—C(5)	−0.8	−0.001	0.66				
H(25)—O(2)—C(5)—C(6)	−171.7	179.9	–				
H(25)—N(2)—C(15)—C(17)	–	–	−0.442				

* Ref. [22].

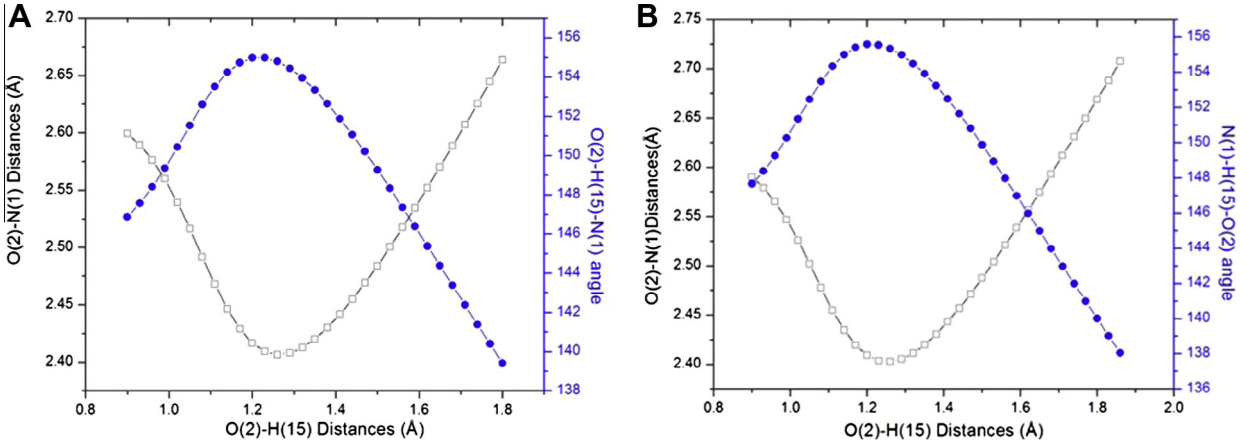

Fig. 2. Variation of O(2)—N(1) distance and O(2)—H(15)—N(1) angle of L2 with O(2)—H(15) distance obtained at B3LYP/6-311 + G(d,p) level of theory: (A) Gas phase; (B) in presence of DMSO solvent.

to 1.86 Å in presence of DMSO solvent. Each time the O(2)—H(15) distance is increased by 0.03 Å and the remaining geometrical parameters are allowed to vary for each fixed O(2)—H(15) distance. The same procedure is also followed for L1. The PECs are plotted using the relative energies (with respect to the lowest energy) as a function of O—H distances (Å) and are given in Fig. 3. Now for generation of the PEC for ESIPT process, we are guided by Franck–Condon principle [30], which tells that the electronic transitions occur so fast that the positions of the nuclei remain unchanged during that transition. Therefore, the transition is vertical in nature. This widely adopted technique to build PEC at excited state [18,21,27–29] provides good agreement with the experimental results [31]. Here we have also generated the PEC for the ESIPT by calculating the vertical transition energies at the TD-DFT-B3LYP/6-311G+(d,p) level for the ground state structures at each point (Fig. 3). In addition, the PEC at excited state is generated by calculating adiabatic transition energy (optimizing at excited state) to know the change in the nature of the curve (between vertical and adiabatic PECs) taking the case of L2 in gas phase as a case study (Fig. 3c).

Fig. 3a shows the potential energy diagram for L2 in gas phase. The ground state PEC clearly shows two shallow minima one at stable O—H distance (1 Å) for enol form and other one at 1.58 Å for keto form. According to the S_0, the enol form is more stable than

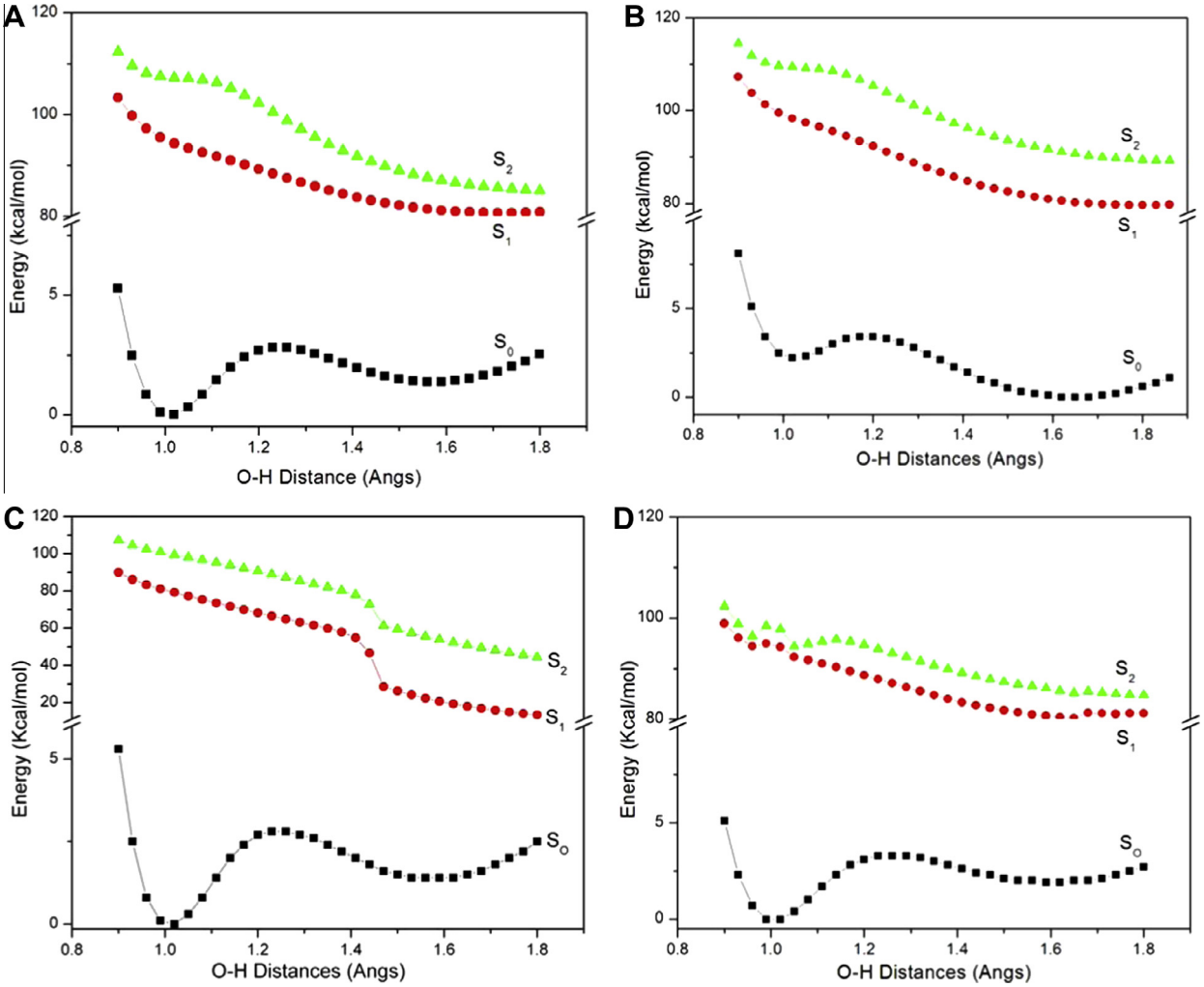

Fig. 3. GSIPT and ESIPT curves of L2 and L1 obtained at B3LYP/6-311 + G(d,p) and TD-DFT-B3LYP/6-311 + G(d,p) levels of theory: (a) Gas phase (vertical excitation) for L2. (b) In presence of DMSO solvent (vertical excitation) for L2. (c) Gas phase (adiabatic excitation) for L2. (d) Gas phase (vertical excitation) for L1.

keto form. But the energy barrier in going from enol to keto form is only 2.8 kcal/mol. Therefore, due to low energy barrier it will be possible to have GSIPT under thermal condition. Interestingly, in both S_1 and S_2 states, the keto form becomes more stable than that of enol form and there is hardly any energy barrier in S_1. Hence, in gas phase ESIPT will occur more likely than GSIPT. In the DMSO solvent phase, S_0 shows (Fig. 3b) two distinct energy minima corresponding to enol and keto forms. Here keto form is more stable than enol form. The energy barrier for the enol to keto conversion is 1.2 kcal/mol in ground state. So, the solvent molecules reduce the energy barrier by ~50% and accelerate the enol to keto conversion process in L2. Note that the energy barrier for the reverse process i.e., keto to enol conversion is 3.4 kcal/mol. It is also quite low to occur at room temperature. Therefore, at ground state there will be always a mixture of keto and enol forms with larger percentage of enol form in gas phase and keto form in solution phase, respectively. In the case of excited state PEC (S_1 and S_2), the curves of S_1 and S_2 are very similar to those of S_1 and S_2 in gas phase. The enol to keto transformation will occur in excited state through almost a barrierless path. Now let us see the difference of the excited state curves generated by vertical and adiabatic transitions (Fig. 3a and c). Both the curves are qualitatively more or less same as both of them show spontaneous conversion (barrierless) from enol form to keto form in the excited state. But they differ quantitatively. The adiabatic excitation energy curve is significantly lower in energy than that of vertical excitation energy curve. It suggests that very large Stokes shift takes place during emission.

We have also considered L1 for further study to know whether the nature of proton transfer in it is same as that in L2. However, we have restricted our study to gas phase only due to certain computational difficulty [32] in solution phase. In L1, there are two equivalent moieties [O(3)—H(26)–N(2) and O(2)—H(25)–N(1)] where intramolecular proton transfer may take place. This is a case of simultaneous double intramolecular proton transfer process. But for simplification we have considered only single proton transfer process occurring in O(3)—H(26)–N(2). The nature of other proton transfer process in O(2)—H(25)–N(1) will be necessarily the same as that of the present case. Similar to L2, here also two minima are observed in S_0, in which the enol form is more stable than keto form (Fig. 3d). The energy barrier in going from enol to keto is found to be 3.3 kcal/mol, which is only slightly larger than that in L2. The S_1 and S_2 plots imply that the intramolecular proton transfer in the enol form of L1 will take place very likely in the excited state.

3.3. Energy and stability

In addition to gas phase, to study the stability of the compounds in solution phases, the optimizations of both keto and enol forms of L1 and L2 are carried out at B3LYP/6-311 + G(d,p) level using PCM

Table 2
Total energy (E_{Total}), HOMO energy (E_{HOMO}), LUMO energy (E_{LUMO}), hardness (η), and dipole moment (μ) of L1 and L2 in gas phase and solution phase studied at B3LYP/6-311 + G(d,p) level.

Compounds	Gaseous		Chloroform		Ethanol		DMSO	
	Enol	Keto	Enol	Keto	Enol	Keto	Enol	Keto
L1								
E_{Total} (a.u)	−1378.9310	−1378.9237	−1378.9513	−1378.9537	−1378.9520	−1378.9574	−1378.9528	−1378.9587
E_{HOMO} (a.u)	−0.21690	−0.2024	−0.22238	−0.20939	−0.2256	−0.21215	−0.22599	−0.21267
E_{LUMO} (a.u)	−0.05039	−0.06402	−0.05252	−0.06718	−0.05407	−0.06797	−0.05427	−0.06815
η (eV)	4.531	3.766	4.622	3.870	4.668	3.923	4.673	3.933
μ (D)	3.830	7.106	5.389	10.286	6.274	11.868	6.422	12.113
L2								
E_{Total} (a.u)	−784.7605	−784.7409	−784.9857	−784.9884	−784.9931	−784.9974	−784.9853	−784.9886
E_{HOMO} (a.u)	−0.2176	−0.2014	−0.22203	−0.20921	−0.2246	−0.21298	−0.22620	−0.21327
E_{LUMO} (a.u)	−0.0487	−0.0589	−0.04951	−0.06353	−0.05075	−0.06594	−0.05226	−0.06612
η (eV)	4.596	3.878	4.695	3.964	4.731	4.001	4.733	4.004
μ (D)	3.305	6.184	4.305	7.156	4.832	7.826	4.816	7.950

Table 3
The experimental and computational vibrational frequencies of L1 and L2 (cm^{-1}).

Assignment	L1		L2	
	Experimental*	B3LYP/6-311 + G(d,p)	Experimental*	B3LYP/6-311 + G(d,p)
O—H	3419	2495	3410	3815
C=N	1608	1616	1597	1674
C—N	1109	1104	1112	1105
C—O	1274	1273	1276	1236
C—O—C	1271	1269	1269	1256
—C≡C—	2123	2113	2117	2253

* Ref. [22].

model in presence of solvents like $CHCl_3$ ($\varepsilon = 4.9$), ethanol ($\varepsilon = 24.55$) and dimethyl sulfoxide ($\varepsilon = 46.68$). Total energy, dipole moment, E_{HOMO}, E_{LUMO} and hardness value (η) of L1 and L2 at gas and solution phases are given in Table 2. The total energy shows that the enol form is more stable than keto form in gas phase. On the other hand, in solution the stability of the keto form is greater than that of enol form. In general, the dipole moment values of L1 and L2 in the keto forms are almost double when compared with those of the enol forms. The values of dihedral angle for L1 and L2 suggest the planar nature of the six membered ring formed by the intramolecular hydrogen bond. Both HOMO and LUMO energy values become more and more negative in going from gaseous phase to solution phase through increasing dielectric constant value. However, the extent of stabilization in HOMO energy is somewhat larger than that of LUMO energy, which results in an increased hardness value.

3.4. FT-IR spectra

The experimentally observed band at 3400 cm^{-1} corresponds to phenolic O—H stretching frequency. The stretching frequency observed at 3294–3284 cm^{-1} range shows the presence of O H···N intramolecular hydrogen bonding in the compounds, L1 and L2 [33]. The C=N stretching frequencies of L1 and L2 are observed at 1612, 1594 cm^{-1}, respectively. The —C≡C group of L1 and L2 shows the stretching frequency at 2123, 2117 cm^{-1} respectively. The appearance of the phenolic C—O band around 1274 cm^{-1} and disappearance of the NH bands are evidence of the existence of enol form in the solid state [34]. The experimental and computed IR frequencies of some selected bands are given in Table 3.

3.5. UV–Visible absorption spectra

The electronic absorption spectra of L1 and L2 are recorded in different solvents like $CHCl_3$, ethanol and DMSO in the region 200–500 nm. The bands observed around 280 and 375 nm correspond

Table 4
Experimental and computed λ_{max}, Oscillator strength (f), Major contributions of L1 and L2.

Compound	Solvent	Experimental λ_{max}	Computed			
			Enol λ_{max} (f)	Major contribution	Keto λ_{max} (f)	Major contribution
L1	Gaseous	–	306.91 (0.2854) 302.44 (0.2101) 268.38 (0.4008)	H-3 → L + 1; H-2 → L H → L H-1 → L H-3 → L + 1; H-2 → L H-1 → L + 1	386.20 382.11	H-1 → L + 1; H → L H-1 → L; H → L + 1
	Chloroform	289 380	303.57 (0.3549) 299.95 (0.2947)	H → L; H-3 → L + 1 H-1 → L; H → L + 1; H-3 → L	384.81 (0.0847) 381.01 (0.2307)	H-1 → L + 1; H → L H-1 → L; H → L + 1
	Ethanol	274 377	299.92 (0.3512) 296.35 (0.2828)	H-1 → L + 1; H → L H-3 → L + 1; H-2 → L H-1 → L; H → L + 1 H-3 → L ; H-2 → L + 1	373.87 (0.09370) 370.13 (0.229)	H-1 → L + 1; H → L H-1 → L; H → L + 1
	DMSO	274 378	300.59 (0.3677) 297.07 (0.3001)	H → L H-1 → L	373.67 (0.0931) 370.09 (0.2442)	H-1 → L + 1; H → L H-1 → L; H → L + 1
L2	Gaseous	 –	301.34 (0.2251) 261.06 (0.29)	H-1 → L + 1; H → L H-1 → L; H → L	392.58 (0.0264) 390.90 (0.0884) 293.50 (0.3831)	H-1 → L; H → L H-2 → L; H-1 → L H → L H-2 → L
	Chloroform	370 291	297.63 (0.321) 259.74 (0.3144)	H → L H-1 → L; H → L H → L + 1	377.86 (0.1634) 289.07 (0.4512)	H → L H-2 → L; H → L + 1
	Ethanol	372 273	295.1 (0.3033) 258.48 (0.306)	H → L H-1 → L; H → L H → L + 1	370.11 (0.1636) 285.65 (0.4413)	H → L H-2 → L; H → L + 1
	DMSO	379 276	295.46 (0.319) 258.69 (0.3119)	H → L H-1 → L; H → L H → L + 1	370.33 (0.1719) 285.95 (0.4544)	H → L H-2 → L; H → L + 1

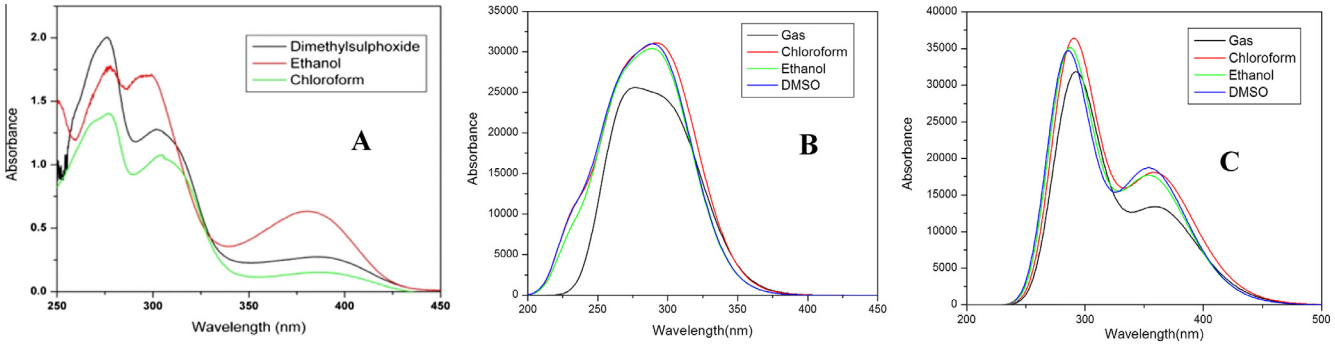

Fig. 4. Experimental (A) and computed UV–Visible spectra of enol (B) and keto (C) forms of L1.

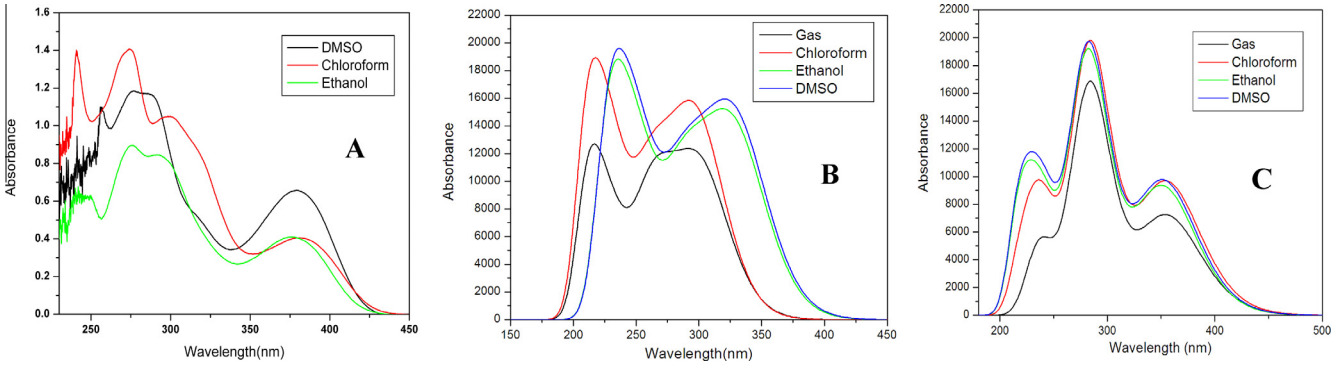

Fig. 5. Experimental (A) and computed UV–Visible spectra of enol(B) and keto(C) forms of L2.

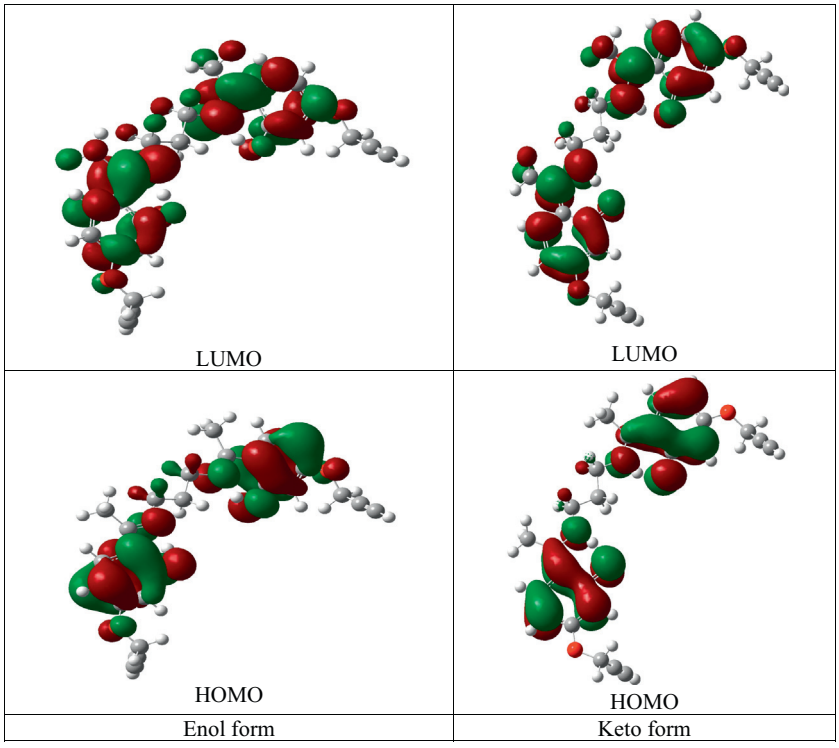

Fig. 6. Frontier molecular orbitals of L1 computed at B3LYP/6-311 + G (d,p) level.

to $\pi-\pi^*$ transitions of benzene ring and azomethine respectively (Table 4). The first twelve spin allowed singlet–singlet excitations for L1 and L2 are calculated by TD-DFT method taking the optimized structures obtained at the same level of theory for gas as well as solution phases ($CHCl_3$, ethanol, DMSO) for keto and enol forms (Figs. 4 and 5). Frontier molecular orbitals of L1 and L2 are given in Figs. 6 and 7. Theoretically calculated λ_{max} values of keto forms are comparable to the corresponding experimental values.

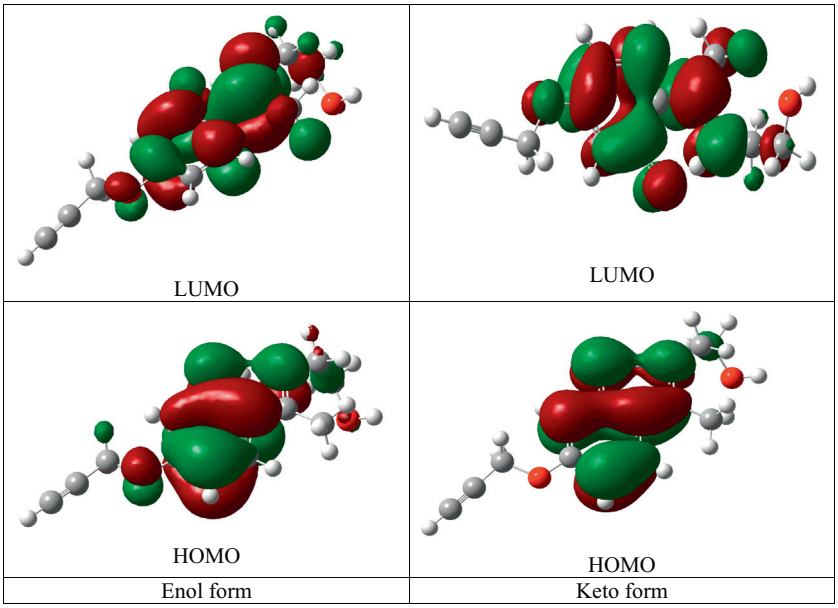

Fig. 7. Frontier molecular orbitals of L2 computed at B3LYP/6-311 + G (d,p) level.

This shows that the compounds L1 and L2 exist in the keto form in solution. This is further supported by the total energy of the compound in solution phase, which is more negative than that of the gas phase (Table 2). In the view of TD-DFT calculation, the excitation energies at 285.9 nm and 370 nm arise from HOMO − 2 → LUMO, HOMO → LUMO + 1 and HOMO → LUMO transition respectively in DMSO for keto form of L2. HOMO orbital arises from sp^2 hybridized orbitals of benzene ring.

4. Conclusions

Density Functional calculation on L1 and L2 compounds reveals that the enol forms are more stable than the corresponding keto forms in gas phase. However, in solution phase, the keto forms are found to be more stable than the respective enol forms. In gas phase, the GSIPT goes through an energy barrier of ~3 kcal/mol (3.3 kcal/mol for L1 and 2.8 for L2) whereas in excited state spontaneous proton transfer will occur. In presence of DMSO solvent, the energy barrier for GSIPT for the enol to keto conversion in ground state reduces to 1.2 kcal/mol. The behavior of ESIPT is more or less same in both gas and solution phases. The calculated vibrational frequencies and UV–Visible spectra are compared with those obtained from experiments. The most important orbital contribution for each electronic transition is assigned.

Acknowledgements

M.A.N. acknowledges the Department of Science and Technology (DST), New Delhi, India (SR/S1/IC-08/2010) for the financial support. One of the authors, B.A. thanks DST for the fellowship. PKC would like to thank DST, New Delhi for the J.C. Bose National Fellowship and SP thanks CSIR, New Delhi for a fellowship.

References

[1] A.V. Pietro, T. Sergio, The challenge of cyclic and acyclic schiff bases and related derivatives, Coord. Chem. Rev. 248 (2004) 1717–2128.
[2] T.S. Baul, S. Bau, D. DeVos, A. Linden, Amino acetate functionalized Schiff base organotin(IV) complexes as anticancer drugs: synthesis, structural characterization, and in vitro cytotoxicity studies, Invest. New Drugs 27 (2009) 419–431.
[3] A.D. Tiwari, A.K. Mishra, B.B. Mishra, B. Maji, S. Bhattacharya, Amino acetate functionalized Schiff base organotin(IV) complexes as anticancer drugs: synthesis, structural characterization, and in vitro cytotoxicity studies, Spectrochim. Acta A 79 (2011) 1050–1056.
[4] J.L. Kraus, B. Belleau, The bioorganic chemistry of N-allyl and N-propargyl substituents in drug interactions with flavin-linked oxidases, Can. J. Chem. 53 (1975) 3141–3144.
[5] A.G. Mavandadi, R.L. Kisliuk, S.F. Queener, Synthesis of classical and a nonclassical 2-amino-4-oxo-6-methyl-5-substituted pyrrolo [2,3-d]pyrimidine antifolate inhibitors of thymidylate synthase, J. Med. Chem. 42 (1999) 2272–2279.
[6] M.F. Rode, A.L. Sobolewski, Photophysics of inter- and intra-molecularly hydrogen-bonded systems: computational studies on the pyrrole–pyridine complex and 2(2′-pyridyl)pyrrole, Chem. Phys. 347 (2008) 413–421.
[7] E. Hadjoudis, M. Vitterakis, I. Moustakali-Mavridis, Photochromism and thermochromism of schiff bases in the solid state and in rigid glasses, Tetrahedron 43 (1987) 1345–1360.
[8] O.-H. Kwon, A.H. Zewail, Double proton transfer dynamics of model DNA base pairs in the condensed phase, Proc. Natl. Acad. Sci. USA 104 (2007) 8703–8708.
[9] K.-L. Han, G.-J. Zhao, Hydrogen Bonding and Transfer in the Excited State, vol. 2, John Wiley & Sons, UK, 2011.
[10] S. Scheiner, Hydrogen Bonding: A Theoretical Perspective, Oxford University Press, New York, 1997.
[11] J. Keck, H.E.A. Kramer, H. Port, T. Hirsch, P. Fischer, G. Rytz, Investigations on polymeric and monomeric intramolecularly hydrogen-bridged UV absorbers of the benzotriazole and triazine class, J. Phys. Chem. 100 (1996) 14468–14475.
[12] P.T. Chou, D. MxMorrow, T.J. Aartsma, M. Kasha, The proton-transfer laser. Galn spectrum and amplificatlon of spontaneous emission of 3-hydroxyflavone, J. Phys. Chem. 88 (1984) 4596–4599.
[13] J. Keck, M. Roessler, C. Schroeder, G.J. Stueber, F. Waiblinger, M. Stein, D. Legourrierec, H.E.A. Kramer, H. Hoier, S. Henkel, P. Fischer, H. Port, T. Hirsch, G. Tytz, P. Hayoz, Ultraviolet absorbers of the 2-(2-hydroxyaryl)-1,3,5-triazine class and their methoxy derivatives: fluorescence spectroscopy and X-ray structure analysis, J. Phys. Chem. B 102 (1998) 6975–6985.
[14] M.L. Martinej, W.C. Cooper, T.T. Chou, A novel excited-state intramolecular proton transfer molecule 10-hydroxybenzo[h] quinoline, Chem. Phys. Lett. 193 (1992) 151–154.
[15] (a) A. Weller, Z Intra molecular proton transfer in excited states, Elektrochem 60 (1956) 1144–1147;
(b) A. Weller, Fast reaction of excited molecules, Prog. React. Kinet. 1 (1961) 187–214.
[16] T. Nishiya, S. Yamauchi, N. Hirota, Y. Fufiwara, M. Itah, Two-step laser excitation study on the proton transfer and anion formation in the intramolecularly hydrogen bonded 7-hydroxy-1-indanone and the related compounds, J. Am. Chem. Soc. 108 (1986) 3880–3884.
[17] I.K. Starzomska, A. Filarowski, M. Rospenk, A. Koll, S. Mlikova, Proton transfer equilibria in Schiff bases with steric repulsion, J. Phys. Chem. A 108 (2004) 2131–2138.
[18] (a) S.P. De, S. Ash, S. Dalai, A. Misra, A DFT-based comparative study on the excited states intramolecular proton transfer in 1-hydroxy-2-naphthaldehyde and 2-hydroxy-3-naphthaldehyde, J. Mol. Struct. (THEOCHEM) 807 (2007) 33–41;

(b) S.P. De, S. Ash, H.K. Bar, D.K. Bhui, P. Sarkar, G.P. Sahoo, A. Misra, DFT based computational study on the excited state intramolecular proton transfer processes in o-hydroxybenzaldehyde, Spectrochim. Acta Part A 71 (2009) 1728–1735;
(c) S. Ash, S.P. De, H. Beg, A. Misra, Excited state intramolecular proton transfer in 3-hydroxychromone: a DFT-based computational study, Mol. Simul. 37 (2011) 914–922.

[19] (a) R.G. Parr, P.K. Chattaraj, Principle of maximum hardness, J. Am. Chem. Soc. 113 (1991) 1854–1855.;
(b) S. Pan, M. Sola, P.K. Chattaraj, On the validity of the maximum hardness principle and the minimum electrophilicity principle during chemical reactions, J. Phys. Chem. A 117 (2013) 1843–1852;
(c) S. Pan, P.K. Chattaraj, Favorable direction in a chemical reaction through the maximum hardness principle, J. Mex. Chem. Soc. 57 (2013) 23–24.

[20] (a) P.K. Chattaraj, S. Sengupta, Popular electronic structure principles in a dynamical context, J. Phys. Chem. 100 (1996) 16126–16130;
(b) P. Fuentealba, Y. Simon- Manso, P.K. Chattaraj, Molecular electronic excitations and the minimum polarizability principle, J. Phys. Chem. A. 104 (2000) 3185.

[21] (a) H. Beg, S.P. De, S. Ash, A. Misra, Use of polarizability and chemical hardness to locate the transition state and the potential energy curve for double proton transfer reaction: a DFT based study, Comput. Theor. Chem. 984 (2012) 13–18;
(b) H. Beg, D. Das, S. Ash, A. Misra, Computation of polarizability, hyper-polarizability and hardness as descriptor for enol–keto tautomerizations of 2-hydroxy pyridines, Comput. Theor. Chem. 1017 (2013) 200–207.

[22] V. Selvarani, B. Annaraj, M.A. Neelakantan, S. Sundaramoorthy, D. Velmurugan, Synthesis and crystal structure of hydroxyacetophenone Schiff bases containing propargyl moiety: Solvent effects on UV–Visible spectra, Spectrochim. Acta A 91 (2012) 329–337.

[23] M.J. Frisch, G.W. Trucks, H.B. Schlegel, G.E. Scuseria, M.A. Robb, J.R. Cheeseman, J.A. Montgomery, T.J. Vreven, K.N. Kudin, J.C. Burant, J.M. Millam, S.S. Iyengar, J. Tomasi, V. Barone, B. Mennucci, M. Cossi, G. Scalmani, N. Rega, G.A. Petersson, H. Nakatsuji, M. Hada, M. Ehara, K. Toyota, R. Fukuda, J. Hasegawa, M. Ishida, T. Nakajima, Y. Honda, O. Kitao, H. Nakai, M. Klene, X. Li, J.E. Knox, H.P. Hratchian, J.B. Cross, C. Adamo, J. Jaramillo, R. Gomperts, R.E. Stratmann, O. Yazyev, A.J. Austin, R. Cammi, C. Pomelli, J.W. Ochterski, P.Y. Ayala, K. Morokuma, G.A. Voth, P. Salvador, J.J. Dannenberg, V.G. Zakrzewski, S. Dapprich, A.D. Daniels, M.C. Strain, O. Farkas, D.K. Malick, A.D. Rabuck, K. Raghavachari, J.B. Foresman, J.V. Ortiz, Q. Cui, A.G. Baboul, S. Clifford, J. Cioslowski, B.B. Stefanov, G. Liu, A. Liashenko, P. Piskorz, I. Komaromi, R.L. Martin, D.J. Fox, T. Keith, M.A. Al-Laham, C.Y. Peng, A. Nanayakkara, M. Challacombe, P.M.W. Gill, B. Johnson, W. Chen, M.W. Wong, C. Gonzalez, J.A. Pople, Gaussian 03; Gaussian Inc.: Wallingford, CT, 2004.

[24] R. Dennington II, T. Keith, J. Millam, GaussView, Version 4.1.2. Semichem Inc., Shawnee Mission, KS, 2007.

[25] S. Miertus, E. Scrocco, J. Tomasi, Electrostatic interaction of a solute with a continuum. A direct utilization of ab initio molecular potentials for the prevision of solvent effects, Chem. Phys. 55 (1981) 117–129.

[26] M.V. Vener, S. Scheiner, Hydrogen bonding and proton transfer in the ground and lowest excited singlet states of o-hydroxyacetophenone, J. Phys. Chem. 99 (1995) 642–649.

[27] A.L. Sobolewski, W. Domcke, Theoretical investigation of potential energy surfaces relevant for excited-state hydrogen transfer in o-hydroxybenzaldehyde, Chem. Phys. 184 (1994) 115.

[28] J. Catalan, J. Palomar, J.L.G. De Paz, Intramolecular proton or hydrogen-atom transfer in the ground and excited states of 2-hydroxybenzoyl compounds, J. Phys. Chem. A 101 (1997) 7914–7921.

[29] S. Maheshwari, A. Chowdhury, N. Sathyamurthy, H. Mishra, H.B. Tripathi, M. Panda, J. Chandrasekhar, Ground and excited state intramolecular proton transfer in salicylic acid: an Ab initio electronic structure investigation, J. Phys. Chem. A 103 (1999) 6257–6262.

[30] E. Condon, A theory of intensity distribution in band systems, Phys. Rev. 28 (1926) 1182–1201.

[31] (a) A.J.A. Aquino, H. Lischka, C. Hättig, Excited-state intramolecular proton transfer: a survey of TDDFT and RI-CC2 excited-state potential energy surfaces, J. Phys. Chem. A 109 (2005) 3201–3208;
(b) A.J.A. Aquino, F. Plasser, M. Barbatti, H. Lischka, Ultrafast excited-state proton transfer processes: energy surfaces and on-the-fly dynamics simulations, Croat. Chem. Acta 82 (2009) 105–114;
(c) S. Jana, S. Dalapati, N. Guchhait, Functional group induced excited state intramolecular proton transfer process in 4-amino-2-methylsulfanylpyrimidine-5-carboxylic acid ethyl ester: a combined spectroscopic and density functional theory study, Photochem. Photobiol. Sci. 12 (2013) 1636–1648.

[32] For L1 we faced difficulty in generating the potential energy curve in presence of DMSO. The problem is due to the hydrogen atom, which is going to make two bonds. But according to UA0 model, the hydrogen is treated implicitly. Then we have tried with universal force field model (UFF). But still we faced convergence problem.

[33] R.M. Silverstein, F.X. Webster, D.J. Kiemle, Spectrometric Identification of Organic Compounds, seventh ed., John Wiley, New York, 2005.

[34] Y. Yeap, S.T. Ha, N. Ishizawa, K. Suda, P.L. Boey, W.A.K. Mahmood, Synthesis, crystal structure and spectroscopic study of para substituted 2-hydroxy-3-methoxybenzalideneanilines, J. Mol. Struct. 658 (2003) 87–99.